Bounding the First Excursion Probability of Linear Structures Subjected to Imprecise Stochastic Loading

Matthias Faes[a,*], Marcos A. Valdebenito[b], David Moens[a], Michael Beer[c,d,e]

[a]*KU Leuven, Department of Mechanical Engineering, Jan De Nayerlaan 5, St.-Katelijne-Waver, Belgium*
[b]*Universidad Tecnica Federico Santa Maria, Dept. de Obras Civiles, Av. España 1680, Valparaiso, Chile*
[c]*Institute for Risk and Reliability, Leibniz Universität Hannover, Callinstr. 34, 30167 Hannover, Germany*
[d]*Institute for Risk and Uncertainty and School of Engineering, University of Liverpool, Peach Street, Liverpool L69 7ZF, UK*
[e]*International Joint Research Center for Engineering Reliability and Stochastic Mechanics, Tongji University, 1239 Siping Road, Shanghai 200092, P.R. China*

Abstract

This paper presents a highly efficient and accurate approach to determine the bounds on the first excursion probability of a linear structure that is subjected to an imprecise stochastic load. Traditionally, determining these bounds involves solving a double loop problem, where the aleatory uncertainty has to be fully propagated for each realization of the epistemic uncertainty or vice versa. When considering realistic structures such as buildings, whose numerical models often contain thousands of degrees of freedom, such approach becomes quickly computationally intractable. In this paper, we introduce an approach to decouple this propagation by applying operator norm theory. In practice, the method determines those epistemic parameter values that yield the bounds on the probability of failure, given the epistemic uncertainty. The probability of failure, conditional on those epistemic parameters, is then computed using the recently introduced framework of Directional Importance Sampling. Two case studies involving a modulated Clough-Penzien spectrum are included to illustrate the efficiency and exactness of the proposed approach.

Keywords: Stochastic loading, First excursion probability, Linear structure, imprecise probabilities, interval analysis

Highlights:

- Effects of imprecision on stochastic loads are considered.
- Reliability of linear dynamical structures is quantified.
- Propagation of epistemic and aleatory uncertainty is decoupled.
- Epistemic uncertainty is propagated using operator norm theorem.

- Probabilities are computed by means of directional importance sampling.

1. Introduction

Dynamic loading acting on structural systems can be seldom described precisely. A classical means for characterizing uncertainty in loading and capturing time correlations is resorting to probability theory and in particular, to stochastic processes, see, e.g. [1, 2]. The framework associated with stochastic processes provides an excellent means for capturing inherent (aleatory) uncertainty. However, issues such as lack of knowledge, conflicting sources of information, vagueness and other epistemic sources of uncertainty may hinder the application of stochastic processes. In such context, imprecise probability (see, e.g. [3]) may offer an appropriate framework for handling both types of uncertainties. While imprecise probability is a versatile tool, it also poses a major challenge from a numerical viewpoint when performing uncertainty quantification, as both sources of uncertainty (aleatory and epistemic) must be propagated to the response of the structural system. In view of such issue, this contribution proposes an approach for dealing with both sources of uncertainties by means of a decoupling strategy, which allows a drastic reduction on numerical efforts when compared to existing alternatives in the literature (see, e.g. [3]). Decoupling is investigated herein for the specific case of the estimation of interval first excursion probability, that quantifies the level of safety of a structure under dynamic loading.

Imprecise probabilistic analysis as described above [4] offers a variety of tools to deal with such "deep" (i.e., a combination of aleatory and epistemic) uncertainty. Following for instance a p-box framework, the epistemically uncertain hyper-parameters of the random parameter distributions are modeled as being interval or fuzzy valued [4], and propagated as such through the numerical simulation model under consideration. It is important to note that such propagation is conducted under the condition that the effects of aleatory and epistemic uncertainty are kept separated. This implies that both sources of uncertainty are usually propagated by means of the so-called double loop approaches, where the outer loop takes care of epistemic uncertainty while the inner loop deals with aleatory uncertainty [5]. Double loop approaches such as e.g., applied in [6] are generally highly accurate, but the corresponding computational cost becomes quickly intractable, especially when industrially sized models are considered. Therefore, a considerable amount of research is focused on finding more efficient techniques for the propagation of deep uncertainty through numerical simulation models. In this context, several authors proposed approaches that rely on the approximation of the interval valued parameters

via series expansion methods (see e.g., [7], [8]) or orthogonal polynomial expansion schemes (see e.g., [9]), effectively enabling propagation without double loop approaches. However, in case the epistemic uncertainty is comparatively large, perturbation approaches are known to be inaccurate [10], a problem that is alleviated by resorting to Chebyshev polynomial based schemes such as presented in [11]. Also efficient surrogate modeling schemes for imprecise probabilistic problems have been proposed using sparse polynomial chaos expansion representations of the model (see e.g., [12, 13]), interval predictor models [14, 15] or variants of the Sobol-Hoeffding decomposition (also known as HDMR representation) of the relation between the epistemic parameters and the probability of failure [16, 17], providing an efficient and accurate approximation of the problem. Yet another type of methods for propagating mixed uncertainty rely on extensions of classical methods for structural reliability, see e.g. [18, 19]. In the context of imprecise probabilistic stochastic processes, such as the ones described in the first paragraph, only very recent initiatives have been undertaken. Gao et al. [20] introduced imprecise random fields where the mean and variance of the field are interval valued. Dannert et al. [21] and Faes and Moens [22] introduced random fields where also the correlation length of the auto-correlation function can be interval valued. Alternative approaches to deal with sources of insufficient data in the description of quantities that are subjected to uncertainty with spatial correlation include methods based on (Bayesian) compressive sampling [23, 24] or Kriging regression models [25].

This paper deals with bounding the first excursion probability of linear systems subjected to an imprecise stochastic excitation. By fully exploiting the linearity in this problem, the method that is introduced in this paper efficiently and effectively computes these bounds by applying operator norm theory. Specifically, operator norms are applied to find those epistemic parameters that yield a bound on the probability of failure a priori, requiring only a single deterministic model evaluation together with the solution of two optimization problems. Then, based on the identified values for the epistemic uncertain parameters, the bounds on the first excursion probability can be obtained by propagating two stochastic processes through the numerical model, which is sped up by applying Directional Importance Sampling [26]. In this paper, the application of the method is examined on the computation of the first excursion probability of a structure that is subjected to a stochastic ground acceleration, which in its turn is modeled as a modulated Clough-Penzien spectrum (see e.g. [1, 2]). A first case study illustrates the method on a single-degree-of-freedom (SDOF) oscillator. This study shows that the method is more efficient than double loop approaches where quasi Monte Carlo or the vertex approach are used for the propagation of the epistemic uncertainty. Furthermore, it is shown that the proposed approach is also

far more accurate than both approaches. The second case study concerns a finite element model of a 6-story building subjected to a modulated Clough-Penzien spectrum. Also in this case, the accuracy and efficiency of the method is illustrated. This paper is structured as follows. Section 2 provides a rigorous formulation of the problem under consideration. Section 3 presents directional Importance Sampling as an extension to the directional sampling method. Section 4 discusses the computation of the reliability of structures subjected to imprecise stochastic loading, both via a traditional double-loop approach, as well as via the presented decoupling approach. Section 5 and 6 provide the illustrative case studies. Finally, Section 7 lists the conclusions of this manuscript.

2. Formulation of the Problem

This section describes the class of problems considered in this contribution, namely calculation of the bounds of first excursion probabilities of linear systems subjected to imprecise stochastic ground acceleration loads. The presented material starts with a formulation considering purely aleatory uncertainty and then, the effects of imprecision are included. Such flow of ideas is selected as the problem of calculating first excursion probabilities in the presence of aleatory uncertainty is already quite involved; thus the consideration of imprecision makes this problem even more challenging.

2.1. Dynamic Analysis

Consider a structural system modeled as linear, elastic and with classical damping. The model possesses n_D degrees-of-freedom, its structural matrices are deterministic, and it is subjected to a stochastic loading $p\left(t\right)$. The equation of motion is [27]:

$$\boldsymbol{M}\ddot{\boldsymbol{x}}(t,\boldsymbol{z})+\boldsymbol{C}\dot{\boldsymbol{x}}\left(t,\boldsymbol{z}\right)+\boldsymbol{K}\boldsymbol{x}\left(t,\boldsymbol{z}\right)=\boldsymbol{\rho}p\left(t,\boldsymbol{z}\right),\ t\in[0,T],\ \boldsymbol{x}(0,\boldsymbol{z})=\dot{\boldsymbol{x}}(t,\boldsymbol{z})=\boldsymbol{0} \tag{1}$$

where $\boldsymbol{x}$, $\dot{\boldsymbol{x}}$ and $\ddot{\boldsymbol{x}}$ are vectors that represent the displacement, velocity and acceleration, respectively, each of dimension $n_D \times 1$; $\boldsymbol{M}$, $\boldsymbol{C}$, and $\boldsymbol{K}$ are the mass, damping and stiffness matrices, respectively, each of dimension $n_D \times n_D$. Vector $\boldsymbol{\rho}$ couples the stochastic loading $p\left(t\right)$ with the corresponding degrees-of-freedom of the structure and its dimension is $n_D \times 1$.

In case where the effects of ground accelerations on a structure are considered, for instance to study the loads induced by earthquakes, the inherent uncertainty associated with this ground acceleration can be described in terms of a stochastic Gaussian processes $P(t)$ [28, 29, 30, 31]. Hereto, let $p(t)$ in Eq. (1) denote a Gaussian ground acceleration acting over a structural system that is dependent on time t.

Without loss of generality, it is assumed in the following that the mean value of this process is zero. In a first approximation, $P(t)$ is regarded as a wide-sense stationary process which can be characterized through its power spectral density $S(\omega)$, where ω denotes circular frequency. The Wiener-Khintchine theorem (see, e.g. [32]) allows for the calculation of the autocorrelation function of a stochastic process from its power spectrum and vice versa based on following Fourier transforms:

$$S(\omega) = \frac{1}{2\pi} \int_{-\infty}^{+\infty} R(\tau) e^{-i\omega\tau} d\tau \tag{2}$$

$$R(\tau) = \int_{-\infty}^{+\infty} S(\omega) e^{i\omega\tau} d\omega \tag{3}$$

with $R(\tau)$ the autocorrelation function with lag τ.

The above discussion assumes that the stochastic process can be modeled as a wide-sense stationary stochastic process. It is clear that this is a simplifying assumption, as loading may in realistic conditions exhibit a non stationary behavior. A possible means for including such effect consists of modulating the stationary stochastic process by means of a deterministic function of time $m(t)$ (see, e.g. [33]). Thus, the autocorrelation function of the stochastic process R^{m} becomes [34]:

$$R^{\mathrm{m}}(t_1, t_2) = m\left(t_1\right) m\left(t_2\right) R^{\mathrm{s}}\left(t_2 - t_1\right) \tag{4}$$

where t_1 and t_2 are two time instants and R^s is the stationary autocorrelation function of the stochastic process, before being modulated.

Samples of the stochastic process as described above can be generated applying the Karhunen-Loève (KL) expansion (see, e.g. [35, 36]). For this purpose, assume that the loading possesses a duration T and that time is discretized such that $t_k = (k-1)\Delta t,\ k = 1, \ldots, n_T$, where Δt is the time step discretization and n_T the number of discrete time steps. Then, the discrete covariance matrix $\mathbf{\Gamma}$ of dimension $n_T \times n_T$ associated with the stochastic loading model becomes:

$$\mathbf{\Gamma} = \begin{bmatrix} m\left(t_1\right) m\left(t_1\right) R^{\mathrm{s}}\left(0\right) & m\left(t_1\right) m\left(t_2\right) R^{\mathrm{s}}\left(t_1 - t_2\right) & \ldots & m\left(t_1\right) m\left(t_{n_T}\right) R^{\mathrm{s}}\left(t_1 - t_{n_T}\right) \\ m\left(t_2\right) m\left(t_1\right) R^{\mathrm{s}}\left(t_2 - t_1\right) & m\left(t_2\right) m\left(t_2\right) R^{\mathrm{s}}\left(0\right) & \ldots & m\left(t_2\right) m\left(t_{n_T}\right) R^{\mathrm{s}}\left(t_2 - t_{n_T}\right) \\ \vdots & \vdots & \ddots & \vdots \\ m\left(t_{n_T}\right) m\left(t_1\right) R^{\mathrm{s}}\left(t_{n_T} - t_1\right) & m\left(t_{n_T}\right) m\left(t_2\right) R^{\mathrm{s}}\left(t_{n_T} - t_2\right) & \ldots & m\left(t_{n_T}\right) m\left(t_{n_T}\right) R^{\mathrm{s}}\left(0\right) \end{bmatrix}$$

Samples of the stochastic ground acceleration can be generated according to the well-known Karhunen-

Loève expansion:

$$\boldsymbol{p}(\boldsymbol{z}) = \boldsymbol{\Psi}\boldsymbol{\Lambda}^{1/2}\boldsymbol{z} \tag{5}$$

where $\boldsymbol{p}$ denotes a $n_T \times 1$ vector containing the sample of the loading; $\boldsymbol{z}$ is a realization of the random variable vector $\boldsymbol{Z}$ which follows a n_{KL}-dimensional standard Gaussian distribution; n_{KL} is the number of terms retained in the KL expansion; $\boldsymbol{\Psi}$ is a $n_T \times n_{KL}$ matrix whose columns contain the eigenvectors associated with the largest n_{KL} eigenvalues of the discrete covariance matrix $\boldsymbol{\Gamma}$; and $\boldsymbol{\Lambda}$ is a $n_{KL} \times n_{KL}$ matrix whose diagonal contains the largest n_{KL} eigenvalues of $\boldsymbol{\Gamma}$. A criterion for selecting the number of terms to be retained in the KL expansion is to find the minimum value of n_{KL} such that $\sum_{p=1}^{n_{KL}} \lambda_p \geq p_v \sum_{p=1}^{n_T} \lambda_p$, where p_v denotes the fraction of the total variance of the underlying stochastic process that is retained by the approximate representation and λ_p is the p-th eigenvalue of $\boldsymbol{\Gamma}$ [37]. For a recent overview of numerical methods to solve the associated Fredholm integral eigenvalue problem, the reader is kindly referred to the overview paper by Betz et al. [38].

In general engineering practice, only a subset of all dynamic responses $\boldsymbol{x}$ of the structure in eq. (1) are of interest for the analysis. These dynamic responses are denoted as $\eta_i(t, \boldsymbol{z}),\ i = 1, \ldots, n_\eta$ and are calculated applying the convolution integral between the corresponding unit impulse response functions $h_i(t),\ i = 1, \ldots, n_\eta$ and the stochastic loading $p(t, \boldsymbol{z})$:

$$\eta_i\left(t, \boldsymbol{z}\right) = \int_0^t h_i\left(t - \tau\right) p\left(t, \boldsymbol{z}\right) d\tau,\ i = 1, \ldots, n_\eta \tag{6}$$

Under the assumption that the responses of interest correspond to a linear combination of the response vector, the unit impulse response functions are calculated as:

$$h_i(t) = \sum_{v=1}^{n_D} \frac{\boldsymbol{\gamma}_i^T \boldsymbol{\phi}_v \boldsymbol{\phi}_v^T \boldsymbol{\rho}}{\boldsymbol{\phi}_v^T \boldsymbol{M} \boldsymbol{\phi}_v} \frac{1}{\omega_{d,v}} e^{-\zeta_v \omega_v t} \sin(\omega_{d,v} t),\ i = 1, \ldots, n_\eta \tag{7}$$

where $\boldsymbol{\phi}_v,\ v = 1, \ldots, n_D$ are the eigenvectors associated with the eigenproblem of the undamped equation of motion; $\omega_v,\ v = 1, \ldots, n_D$ are the natural frequencies of the system; $\zeta_v,\ v = 1, \ldots, n_D$ are the corresponding damping ratios; $\omega_{d,v} = \omega_v \sqrt{(1 - \zeta_v^2)},\ v = 1, \ldots, n_D$ are the damped frequencies; and $\boldsymbol{\gamma}_i$ is a constant vector such that $\eta_i = \boldsymbol{\gamma}_i^T \boldsymbol{x}$. It should be noted that the contribution of higher order modes to the unit impulse response function in Eq. (7) is negligible for several cases of practical interest [27].

In view of the excitation model introduced in Eq. (5), the dynamic response of interest evaluated at

time t_k is:

$$\eta_i(t_k, \boldsymbol{z}) = \sum_{l_1=1}^{k} \Delta t \epsilon_{l_1} h_i(t_k - t_{l_1}) \left(\sum_{l_2=1}^{n_{KL}} \psi_{l_1,l_2} \sqrt{\lambda_{l_2}} z_{l_2} \right) \tag{8}$$

$$= \boldsymbol{a}_{i,k}^T \boldsymbol{z}, \ i = 1, \ldots, n_\eta, \ k = 1, \ldots, n_T \tag{9}$$

where ψ_{l_1,l_2} is the (l_1, l_2)-th element of matrix $\boldsymbol{\Psi}$; $\boldsymbol{a}_{i,k}$ is a vector of dimension $n_{KL} \times 1$ such that:

$$\boldsymbol{a}_{i,k} = \begin{bmatrix} \sum_{l_1=1}^{k} \Delta t \epsilon_{l_1} h_i(t_k - t_{l_1}) \psi_{l_1,1} \sqrt{\lambda_1} \\ \sum_{l_1=1}^{k} \Delta t \epsilon_{l_1} h_i(t_k - t_{l_1}) \psi_{l_1,2} \sqrt{\lambda_2} \\ \vdots \\ \sum_{l_1=1}^{k} \Delta t \epsilon_{l_1} h_i(t_k - t_{l_1}) \psi_{l_1,n_{KL}} \sqrt{\lambda_{n_{KL}}} \end{bmatrix} \tag{10}$$

and ϵ_{l_1} is a coefficient depending on the numerical integration scheme used in the evaluation of the convolution integral. For the case where the trapezoidal integration rule [39] is chosen, $\epsilon_{l_1} = 1/2$ if $l_1 = 1$ or $l_1 = k$; otherwise, $\epsilon_{l_1} = 1$.

2.2. Precise reliability analysis

Structural systems subjected to a stochastic loading as described above exhibit an uncertain response. A possible means for quantifying such uncertainty consists of calculating the first excursion probability, which measures the probability that any of the responses of interest $\eta_i(t), \ i = 1, \ldots, n_\eta$ exceeds a prescribed threshold level $b_i, \ i = 1, \ldots, n_\eta$ within the duration T of the stochastic excitation. This failure criterion is cast in terms of the so-called performance function, which is equal to:

$$g(\boldsymbol{z}) = 1 - \max_{i=1,\ldots,n_\eta} \left(\max_{k=1,\ldots,n_T} \left(\frac{|\eta_i(t_k, \boldsymbol{z})|}{b_i} \right) \right) \tag{11}$$

where $|\cdot|$ denotes the absolute value. From this equation, note that the term $|\eta_i(t_k, \boldsymbol{z})|/b_i$ represents the *normalized demand*, which measures how close the response of interest lies to the allowable threshold in a dimensionless manner [40]. Thus, whenever the maximum normalized demand (retrieved by $\max(\cdot)$ in eq. (11)) exceeds unity, failure takes place. The above formulation of the performance function corresponds to a classical series event (see, e.g. [41]).

As such, the first excursion probability is written in terms of the following integral [32, 41, 42]:

$$P_f = \int_{\boldsymbol{z}\in\mathbb{R}^{n_{KL}}} I_F\left(\boldsymbol{z}\right) f_{\boldsymbol{Z}}\left(\boldsymbol{z}\right) d\boldsymbol{z} \tag{12}$$

where $f_{\boldsymbol{Z}}\left(\cdot\right)$ is standard Gaussian probability density function in n_{KL} dimensions; and $I_F\left(\cdot\right)$, is an indicator function whose value is equal to one in case $g(\boldsymbol{z}) < 0$ and zero otherwise. It is noted that the probability integral in Eq. (12) usually comprises a high number of dimensions, as n_{KL} may be in the order of hundreds or thousands, while the indicator function is known point-wise only for specific realizations $\boldsymbol{z}$ of $\boldsymbol{Z}$. Therefore, such an integral cannot be solved analytically; however, lower/upper bounds [43] or approximate solutions [44] exist in certain cases. For more general cases, simulation methods appear to be the only feasible means for evaluating the failure probability, see e.g. [45].

2.3. Effects of Imprecision on Stochastic Loading and First Excursion Probability

The characterization of the stochastic process in terms of its power spectral density or autocorrelation function and a modulating function as described above usually relies on a prescribed model, which in its turn depends on a number of parameters, grouped in a vector $\boldsymbol{\theta}$. Without loss of generality, in this paper we consider the modulated Clough-Penzien (CP) autocorrelation function (see also Appendix A). The parameters that determine the auto-correlation function $R^m(t_1, t_2)$ in this case reflect some specific characteristics of the process, such as dominant frequencies, amplitude, etc. Naturally, when setting the model, there might be considerable uncertainty on the precise values of these parameters [46] arising due to issues such as lack of knowledge, vagueness, conflicting information sources, etc., especially given the fact that these parameters may be highly sensitive to specific site conditions. For instance, considering Table A.7, a selection of the appropriate parameters has to be made based on the classification of the soil being *Firm*, *Medium* or *Soft*. As an illustration of the effect of this imprecision, figure 1 shows the power spectrum corresponding to these three classifications of the soil and a spectral intensity $S_0 = 0.05$ m^2/s^3. The figure furthermore shows a realization of the stochastic process corresponding to each of these spectra, with parameters of the modulation equal to $c_1 = 0.14$, $c_2 = 0.16$ (see details in Appendix A), where $\boldsymbol{z}$ is taken to be the same for the three processes. As is clear from this figure, the classification of the soil has a large impact on the representation of the base excitation that is imposed on the structure under consideration.

In such scenario, non-traditional models for uncertainty quantification appear as a natural choice for characterizing the parameters $\boldsymbol{\theta}$ of the stochastic loading [4, 10], as they provide the analyst with

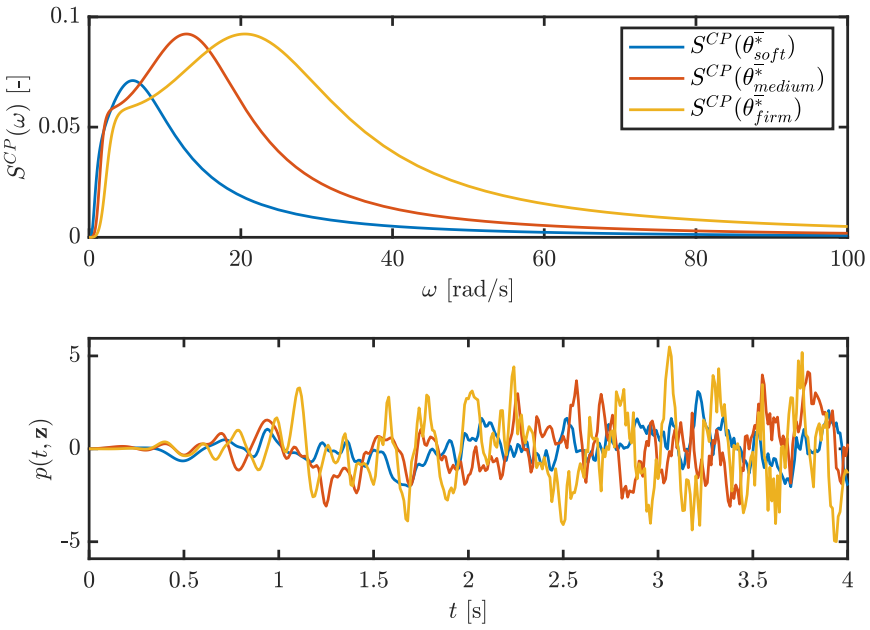

Figure 1: Clough-Penzien spectra corresponding to a soft, medium or firm soil as well as one realisation from the stochastic process corresponding to these spectra.

more objective and robust tools to asses the bounds on the estimated reliability of the structure, based on epistemic uncertainty that is present on the parameters of the stochastic process definition. In this paper, the uncertainty of each of these parameters is characterized as an interval vector $\boldsymbol{\theta}^I$, as intervals require only very few data points to make an objective worst-case estimate of the bounds on the reliability [10]. Furthermore, recent developments allow for estimating robust interval bounds given only limited data (see e.g., [47, 48]). In the following intervals are denoted with apex I, e.g. $\boldsymbol{\theta}^I$ denotes the interval associated with $\boldsymbol{\theta}$. In the example of the modulated CP auto-correlation function, $\boldsymbol{\theta}^I$ is defined as $\boldsymbol{\theta}^I = [\omega_g^I, \omega_f^I, \zeta_g^I, \zeta_f^I, S_0^I, c_1^I, c_2^I]$, which can geometrically be represented as a 7-dimensional hyper-rectangular input space (please see Appendix A for the physical interpretation of these parameters).

The fact that the input parameters of the stochastic loading model are described by means of intervals has important implications on the evaluation of the structural reliability of the model under consideration. In particular, both the loading and the responses of interest of the structural system become interval stochastic processes, as described in [22]. This implies in turn that the performance function becomes interval valued, which causes the failure probability to become interval valued as well. This implies that both the lower bound $\underline{P}_f$ and upper bound $\overline{P}_f$ of the interval associated the failure

probability p_F^I must be determined, which leads to the following two optimization problems:

$$\underline{P}_f = \min_{\boldsymbol{\theta}\in\boldsymbol{\theta}^I}\left(P_f(\boldsymbol{\theta})\right) = \min_{\boldsymbol{\theta}\in\boldsymbol{\theta}^I}\left(\int_{\boldsymbol{z}\in\mathbb{R}^{n_{KL}}} I_F\left(\boldsymbol{z},\boldsymbol{\theta}\right) f_{\boldsymbol{Z}}\left(\boldsymbol{z}\right) d\boldsymbol{z}\right) \tag{13}$$

$$\overline{P}_f = \max_{\boldsymbol{\theta}\in\boldsymbol{\theta}^I}\left(P_f(\boldsymbol{\theta})\right) = \max_{\boldsymbol{\theta}\in\boldsymbol{\theta}^I}\left(\int_{\boldsymbol{z}\in\mathbb{R}^{n_{KL}}} I_F\left(\boldsymbol{z},\boldsymbol{\theta}\right) f_{\boldsymbol{Z}}\left(\boldsymbol{z}\right) d\boldsymbol{z}\right) \tag{14}$$

The calculation of the bounds associated with the failure probability can be extremely demanding from a numerical viewpoint. On one hand, the calculation of the failure probability for a fixed value of the parameters associated with the stochastic process is quite costly, even when highly efficient methods such as Directional Importance Sampling (as described in the forthcoming section) are applied. On the other hand, solving the associated optimization problems is far from trivial, as it constitutes a double loop problem, where the inner loop comprises probability calculation, while the outer loop explores the possible values that the parameters $\boldsymbol{\theta}$ may assume. As such, a full propagation of the stochastic process towards the first excursion probability has to be performed. Hence, apart from considering near-trivial simulation models, such computation is intractable without resorting to surrogate modelling strategies [49].

Such task is carried out as follows in this work: Section 3 addresses the issue of the failure probability whenever the stochastic loading process is characterized precisely (that is, for a crisp value of $\boldsymbol{\theta}$), while in Section 4, the effect of imprecision on the stochastic loading model is explicitly included in the analysis and the bounds on the interval failure probability are calculated efficiently and accurately with the help of the operator norm theorem.

3. Directional importance sampling

3.1. Context

This section presents Directional Importance Sampling (DIS), which is a simulation approach that allows calculating first excursion probabilities of linear structural systems subject to Gaussian loading [26]. In the following, it is assumed that the parameters $\boldsymbol{\theta}$ associated with the stochastic loading model can be regarded as deterministic. In this context, note that the estimation of such first excursion probabilities is not trivial (even when precise probabilistic models are considered) and hence, DIS plays a fundamental role for reliability assessment within the proposed framework.

3.2. Basic formulation

Directional sampling (see e.g., [50], [51]) consists of exploring the input space associated with the stochastic loading by random samples of a unit direction vector amplified by a length factor. This corresponds to a polar representation, as discussed in detail in [52]. Thus, the realization $\boldsymbol{z}$ is represented as:

$$\boldsymbol{z} = r\boldsymbol{u} \tag{15}$$

where $\boldsymbol{u}$ is a unit vector pointing towards $\boldsymbol{z}$, that is:

$$\boldsymbol{u} = \frac{\boldsymbol{z}}{\|\boldsymbol{z}\|_2} \tag{16}$$

where $\|\cdot\|_2$ denotes the Euclidean norm; and r is the Euclidean norm of $\boldsymbol{z}$, that is $r = \|\boldsymbol{z}\|_2$. Thus, the failure probability integral in Eq. (12) is expressed as:

$$P_f = \int_r \int_{\boldsymbol{u}} I_F\left(r\boldsymbol{u}\right) f_R\left(r\right) f_{\boldsymbol{U}}\left(\boldsymbol{u}\right) d\boldsymbol{u} dr \tag{17}$$

where $f_{\boldsymbol{U}}\left(\boldsymbol{u}\right)$ is the uniform probability distribution over a hypersphere and $f_R(r)$ is the probability density function associated with r. It is readily seen that applying the formula for change of variables for probability distributions [53], $f_R(r) = 2r f_{\chi^2_{n_T}}(r^2)$, where $f_{\chi^2_{n_T}}(r^2)$ is the Chi-squared probability density function of n_T degrees-of-freedom (recall that r^2 follows a Chi-squared distribution of n_T degrees-of-freedom as it is the sum of the squares of n_T standard Gaussian variables).

Direct estimation by means of simulation of Eq. (17) may not be efficient: as failure probabilities are usually low (e.g. 10^{-3} or less), the associated estimator may exhibit a large variability. Such issue can be alleviated by introducing a suitable importance sampling density function $f_{\boldsymbol{U},IS}\left(\boldsymbol{u}\right)$, which leads to the following expression for the failure probability integral:

$$P_f = \int_r \int_{\boldsymbol{u}} I_F\left(r\boldsymbol{u}\right) f_R\left(r\right) \frac{f_{\boldsymbol{U}}\left(\boldsymbol{u}\right)}{f_{\boldsymbol{U},IS}\left(\boldsymbol{u}\right)} f_{\boldsymbol{U},IS}\left(\boldsymbol{u}\right) d\boldsymbol{u} dr \tag{18}$$

The above expression corresponds to a Directional Importance Sampling (DIS) strategy for calculating the failure probability and it can be efficiently estimated by means of random sampling given that the importance sampling density function $f_{\boldsymbol{U},IS}\left(\boldsymbol{u}\right)$ is selected appropriately. This issue is discussed in the following.

3.2.1. Failure domain and its geometry

As discussed in [54], the safe and failure domains associated with the first excursion probability of a linear structure subject to Gaussian excitation are separated by a collection of hyperplanes. Such information provides valuable information for selecting $f_{\boldsymbol{U},IS}(\boldsymbol{u})$.

Consider the so-called positive elementary failure domain ${F_{i,k}}^{+}$, which is the set that collects all realizations $\boldsymbol{z}$ such that the response η_i exceeds its corresponding threshold b_i at the time instant t_k. In view of linearity of the response of interest with respect to $\boldsymbol{z}$ as shown in Eq. (8), it is noted that the set ${F_{i,k}}^{+}$ is bounded by a hyperplane, that is:

$$ {F_{i,k}}^{+} = \left\{ \boldsymbol{z} \in \mathbb{R}^{n_{KL}} : \boldsymbol{a}_{i,k}^{T} \boldsymbol{z} \geq b_i \right\} \tag{19} $$

In a similar manner, the negative elementary failure domain ${F_{i,k}}^{-}$, in which the response of interest η_i exceeds the threshold $-b_i$ at the time instant t_k, is also bounded by a hyperplane:

$$ {F_{i,k}}^{-} = \left\{ \boldsymbol{z} \in \mathbb{R}^{n_{KL}} : \boldsymbol{a}_{i,k}^{T} \boldsymbol{z} \leq -b_i \right\} \tag{20} $$

The union of positive and negative elementary failure domains ${F_{i,k}}^{+}$ and ${F_{i,k}}^{-}$, respectively, forms the elementary failure domain $F_{i,k}$. In addition, the overall failure event F is formed by the union of elementary failure events (see, e.g. [41]).

$$ F = \bigcup_{i=1}^{n_\eta} \bigcup_{k=1}^{n_T} F_{i,k} \tag{21} $$

Note that the failure event F contains all possible random excitations that cause a first excursion. These elementary failure domains are represented schematically in Figure 2.

As the elementary failure events $F_{i,k}$ are bounded by hyperplanes, their individual probability of occurrence is completely characterized by the reliability indexes $\beta_{i,k},\ i = 1, \ldots, n_\eta,\ k = 1, \ldots, n_T$. These indexes are equal to [54, 55]:

$$ \beta_{i,k} = \frac{b_i}{\|\boldsymbol{a}_{i,k}\|} \tag{22} $$

Figure 2 provides a schematic representation of the reliability indexes. From this figure, it is easy to see that these indexes are actually equal to the Euclidean norm of the design points associated with each

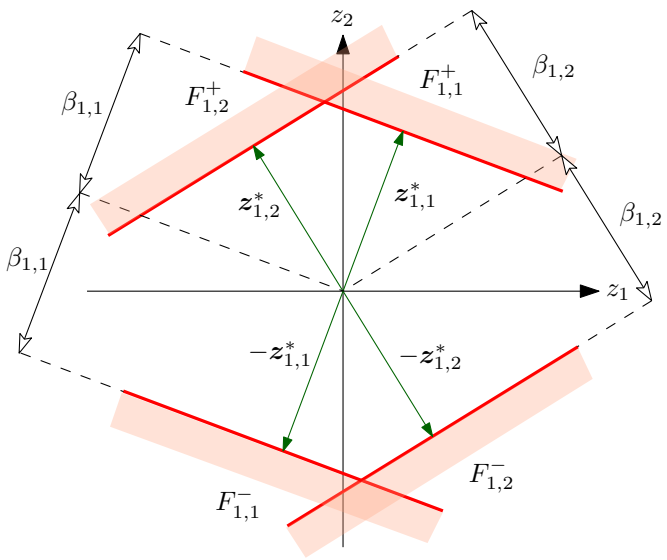

Figure 2: Failure domain for the case where $n_{KL} = 2$.

elementary failure domain (please see [54, 55] for details on the definition of the design point). Hence, the probability of occurrence of each of the elementary failure events is given by:

$$P\left[F_{i,k}\right] = 2\Phi\left(-\beta_{i,k}\right) \tag{23}$$

where $P[\cdot]$ denotes probability and $\Phi\left(\cdot\right)$ represents the standard normal cumulative density function. The summation $\hat{P}_f$ of the probability of occurrence of each elementary failure event:

$$\hat{P}_f = 2\sum_{i=1}^{n_\eta}\sum_{k=1}^{n_T}\Phi\left(-\beta_{i,k}\right) \tag{24}$$

provides an upper bound for the sought first excursion probability [41, 55], that is $P_f \leq \hat{P}_f$.

As the elementary failure domains are bounded by hyperplanes, it is possible to deduce some analytic expressions associated with them. For example, the probability density associated with a direction $\boldsymbol{u}$ in the standard normal space given that the elementary failure event $F_{i,k}$ occurs, which is denoted as $f_{\boldsymbol{U}}\left(\boldsymbol{u}|F_{i,k}\right)$, can be calculated in closed form by virtue of Bayes' theorem, yielding [26, 52]:

$$f_{\boldsymbol{U}}\left(\boldsymbol{u}|F_{i,k}\right) = \frac{f_{\boldsymbol{U}}(\boldsymbol{u})P\left[F_{i,k}|\boldsymbol{u}\right]}{P[F_{i,k}]} \tag{25}$$

The term $P\left[F_{i,k}|\boldsymbol{u}\right]$ expresses the probability of occurrence of the elementary failure domain $F_{i,k}$ conditioned on the unit direction $\boldsymbol{u}$. It can be readily demonstrated that such probability can be solved in

closed form (see detailed deduction in [26]), leading to:

$$f_{\boldsymbol{U}}\left(\boldsymbol{u}|F_{i,k}\right)=\frac{f_{\boldsymbol{U}}\left(\boldsymbol{u}\right)\left(1-F_{X^2_{nT}}\left(C_{i,k}(\boldsymbol{u})^2\right)\right)}{P[F_{i,k}]} \tag{26}$$

where $F_{\chi^2_{nT}}(\cdot)$ corresponds to the Chi-squared cumulative density function with n_T degrees-of-freedom and $C_{i,k}(\boldsymbol{u})$ corresponds to the Euclidean norm of the vector lying between the origin of the standard normal space and the intersection of the boundary of $F_{i,k}$ with the ray along the direction $\boldsymbol{u}$. In view of linearity of the response, it is straightforward to demonstrate that $C_{i,k}(\boldsymbol{u})$ is equal to [26]:

$$C_{i,k}(\boldsymbol{u})=\frac{b_i}{|\eta_i(t_k,\boldsymbol{u})|} \tag{27}$$

As $f_{\boldsymbol{U}}\left(\boldsymbol{u}|F_{i,k}\right)$ is known in closed form, it provides valuable information for setting an importance sampling density function $f_{\boldsymbol{U},IS}\left(\boldsymbol{u}\right)$. In fact, the latter density function is selected as a weighted summation of the probability density function associated with $\boldsymbol{u}$ conditioned on the different elementary failure domains [55], that is:

$$f_{\boldsymbol{U},IS}\left(\boldsymbol{u}\right)=\sum_{i=1}^{n_\eta}\sum_{k=1}^{n_T}w_{i,k}f_{\boldsymbol{u}}\left(\boldsymbol{u}|F_{i,k}\right) \tag{28}$$

where $w_{i,k}$ is a weight associated with the elementary failure domain $F_{i,k}$, which is selected as [56]:

$$w_{i,k}=\frac{P[F_{i,k}]}{\sum_{l=1}^{n_\eta}\sum_{m=1}^{n_T}P[F_{l,m}]} \tag{29}$$

Taking into account all previous results, the importance sampling density function $f_{\boldsymbol{U},IS}\left(\boldsymbol{u}\right)$ reduces to:

$$f_{\boldsymbol{U},IS}\left(\boldsymbol{u}\right)=\frac{f_{\boldsymbol{U}}\left(\boldsymbol{u}\right)}{\hat{P}_f}\sum_{i=1}^{n_\eta}\sum_{k=1}^{n_T}\left(1-F_{\chi^2_{n_T}}\left(C_{i,k}(\boldsymbol{u})^2\right)\right) \tag{30}$$

The main advantage of the above importance sampling density function is that it ensures that samples of the direction vector $\boldsymbol{u}$ which are highly relevant for the failure probability calculation are drawn frequently within the context of simulation.

3.2.2. Estimator of first excursion probability

The importance sampling density function proposed in Eq. (30) applied over Eq. (18) leads to the following estimator for the first excursion probability:

$$\tilde{P}_f^{\mathrm{DIS}} \approx \frac{\hat{P}_F}{N} \sum_{j=1}^{N} \frac{1 - F_{\chi^2_{n_T}} \left(\left(C_{\min} \left(\boldsymbol{u}^{(j)} \right) \right)^2 \right)}{D \left(\boldsymbol{u}^{(j)} \right)} \tag{31}$$

where $\boldsymbol{u}^{(j)}$ are N independent, identically distributed samples that follow $f_{\boldsymbol{U},IS}(\boldsymbol{u})$ and where:

$$C_{\min} \left(\boldsymbol{u}^{(j)} \right) = \min \left(C_{i,k} \left(\boldsymbol{u}^{(j)} \right) \right) \tag{32}$$

with $i = 1, \ldots, n_\eta$ and $k = 1, \ldots, n_T$, and:

$$D \left(\boldsymbol{u}^{(j)} \right) = \sum_{i=1}^{n_\eta} \sum_{k=1}^{n_T} \left(1 - F_{\chi^2_{n_T}} \left(C_{i,k} \left(\boldsymbol{u}^{(j)} \right)^2 \right) \right) \tag{33}$$

Samples of $\boldsymbol{u}$ distributed according to $f_{\boldsymbol{U},IS}(\boldsymbol{u})$ can be generated using the approach described in [26, 57]. This approach comprises the following basic steps:

- Generate a sample $\boldsymbol{z}$ that follows a standard Gaussian distribution in n_T dimensions.
- Select an elementary failure domain $F_{i^\star,k^\star}$ with probability proportional to its weight $w_{i^\star,k^\star}$.
- Generate a sample $\boldsymbol{z}^\star$ which follows a standard Gaussian distribution conditioned on the failure event $F_{i^\star,k^\star}$. Such sample is generated by manipulating the projection of $\boldsymbol{z}$ onto $F_{i^\star,k^\star}$ [55].
- The sought sample of the direction is chosen as the unit vector pointing towards $\boldsymbol{z}^\star$, that is $\boldsymbol{u} = \boldsymbol{z}^\star / ||\boldsymbol{z}^\star||_2^2$.

For a detailed description of the approach for generating a sample of $\boldsymbol{u}$ distributed according to $f_{\boldsymbol{U},IS}(\boldsymbol{u})$, it is referred to [26, 57].

Numerical experience as reported in [26] suggests that the probability estimator in eq. (31) is highly efficient, as it allows estimating small failure probabilities (10^{-3} or less) with high accuracy (that is, coefficient of variation smaller than 10%) and high efficiency (that is, a few hundred samples).

4. Reliability of structures subjected to imprecise stochastic loading

This section focuses on the calculation of the failure probability for the case where the effects of imprecision are included in the description of the stochastic loading process by the interval vector $\boldsymbol{\theta}^I$. A naive approach would involve solving Eq. (13) and (14) directly following a double-loop approach. However, since we consider linear structures, the double loop problem described by Eq. (13) and (14) can be decoupled by determining those parameter values in $\boldsymbol{\theta}^I$ that yield $\overline{P}_f$ and $\underline{P}_f$ *a priori* using operator norm theory.

4.1. General framework

The decoupling of the double loop is based on the operator norm theorem, which states that for any continuous map $A : \mathbb{R}^{n_{KL}} \mapsto \mathbb{R}^{n_T}$ it holds that there exists a real number c and arbitrary vector $v \in \mathbb{R}^{n_{KL}}$ such that:

$$||Av||_{p^{(1)}} \leq |c| \cdot ||v||_{p^{(2)}} \tag{34}$$

where $||\bullet||_p$ denotes a norm on the vector spaces $\mathbb{R}^{n_{KL}}$ and $\mathbb{R}^{n_T}$ and $p^{(i)} \geq 1$ constructs a particular $\mathcal{L}_p$ norm according to:

$$||v||_p = \left(\sum_{i=1}^{n_{KL}} |v_i|^p \right)^{1/p} \tag{35}$$

Note that the norms on the vector spaces on both sides of the equation are not necessarily equal. Physically speaking, Eq.(34) states that the *length* of the vector v can maximally be increased by a factor c as a result of applying the linear mapping described by A. The operator norm $||A||_{p^{(1)},p^{(2)}}$ of the linear map A describes how much A lengthens vectors $v \in \mathbb{R}^{n_{KL}}$in the maximum case, and is defined as:

$$||A||_{p^{(1)},p^{(2)}} = \inf \left\{ c \geq 0 : ||Av||_{p^{(1)}} \leq |c| \cdot ||v||_{p^{(2)}} \quad \forall v \in \mathbb{R}^{n_{KL}} \right\} \tag{36}$$

The operator norm on A can equivalently be defined as:

$$||A||_{p^{(1)},p^{(2)}} = \sup \left\{ \frac{||Av||_{p^{(1)}}}{||v||_{p^{(2)}}} : v \in \mathbb{R}^{n_{KL}} \text{ with } v \neq 0 \right\} \tag{37}$$

Note that the definition of the vector spaces as $\mathbb{R}^{n_{KL}}$ and $\mathbb{R}^{n_T}$ is only made to highlight the link with the previous section. In fact, this theorem holds for all normed spaces on $\mathbb{R}$ or $\mathbb{C}$, as long as the map A is continuous.

In the context of determining the bounds on the probability of failure of a linear structure, subjected

to an imprecise stochastic load, A_i is defined as $A_i(\boldsymbol{\theta}) = [\boldsymbol{a}_{i,1}^T(\boldsymbol{\theta}); \boldsymbol{a}_{i,2}^T(\boldsymbol{\theta}); \ldots; \boldsymbol{a}_{i,n_T}^T(\boldsymbol{\theta})]$, i.e., the column stacking of the $\boldsymbol{a}_{i,k}$ vectors for the $k = 1, ..., n_T$ time instants (as defined in Eq. (10)). In this case, Eq. (34) can be rewritten as:

$$||A_i(\boldsymbol{\theta})\,\boldsymbol{z}||_{p^{(1)}} \leq |c_i(\boldsymbol{\theta})| \cdot ||\boldsymbol{z}||_{p^{(2)}} \tag{38}$$

which is by virtue of Eq. (8) equivalent to:

$$||\eta_i(t, \boldsymbol{\theta}, \boldsymbol{z})||_{p^{(1)}} \leq |c_i(\boldsymbol{\theta})| \cdot ||\boldsymbol{z}||_{p^{(2)}} \tag{39}$$

where $\eta_i(t, \boldsymbol{z})$ denotes the i^{th} dynamic response as a function of t, and $\boldsymbol{z}$ are the i.i.d. Gaussian variables stemming from the KL expansion in Eq. (5). The computation of the operator norm $||A||_{p^{(1)},p^{(2)}}$ is in this case related to the choice of the type of $\mathcal{L}_p$ norm that is selected on both sides of the equation, which is highly case-dependent. In the specific case of bounding the probability of failure described as the first excursion probability of a linear dynamic system, the analysis is mainly driven by the extreme responses $\eta_i(t, \boldsymbol{\theta}, \boldsymbol{z})$ within the duration T of the stochastic excitation. As such, the operator norm should be defined such that it describes the maximum amplification of the *length* of $\boldsymbol{z}$ towards the maximum values in $\eta_i(t, \boldsymbol{\theta}, \boldsymbol{z})$, as those drive the calculation of the first excursion probability. Therefore, following problem is considered:

$$||\eta_i(t, \boldsymbol{\theta}, \boldsymbol{z})||_{\infty} \leq |c_i(\boldsymbol{\theta})| \cdot ||\boldsymbol{z}||_2 \tag{40}$$

The choice for an $\mathcal{L}_\infty$ norm is motivated by the notion that those values in $\boldsymbol{\theta}$ that yield the most extreme structural responses are of highest interest, as these extremes in the responses are the ones that predominantly drive the probability of failure. Concerning the right hand side, the $\mathcal{L}_2$ norm is selected as it can be loosely defined as the energy content in the random variables. It should be noted that the latter is in fact a constant value (in average), as $\boldsymbol{z}$ is by construction a set of i.i.d. standard normal random variables. As a matter of fact, the selection of the norm on $||\boldsymbol{z}||$ does not matter, as the vector in case of a Gaussian stochastic process is always dictated by a standard normal distribution (as presented in the context of this work). In this case, it can be shown that $||A||_{p^{(1)},p^{(2)}}$ can be computed as [58]:

$$||A||_{p^{(1)},p^{(2)}} = \max_l ||A_{i,l:}(\boldsymbol{\theta})||_2 \tag{41}$$

where the subscript $l:$ denotes taking the l^{th} row of the matrix $A_i(\boldsymbol{\theta})$. As such, $||A||_{p^{(1)},p^{(2)}}$ is computed as the maximum $\mathcal{L}_2$ norm of a row of $A_i(\boldsymbol{\theta})$. Physically speaking, $\boldsymbol{\theta}$ is a measure for the best possible

amplification of the energy contained in $\boldsymbol{z}$ to the extreme values of the dynamic response $\eta_i(t, \boldsymbol{\theta}, \boldsymbol{z})$ under consideration.

4.2. Bounds on the probability of failure using operator norm theory

To determine the bounds on P_f without resorting to a double loop optimization procedure, the operator norm framework that was explained in the previous section can be applied. Indeed, since the operator norm describes the elongation of $\boldsymbol{z}$ to the largest responses of the system, it can be used to determine those values of $\boldsymbol{\theta}$ that provide the largest possible elongation of $\boldsymbol{z}$ by min/maximizing the operator norm with respect to $\boldsymbol{\theta}$.

First, consider a structure with a single dynamic response $\eta(t, \boldsymbol{z})$ that drives the computation of P_f. In this case, to determine which values in $\boldsymbol{\theta}^I$ yield respectively $\overline{P}_f$ and $\underline{P}_f$, following optimization problems have to be solved:

$$\theta^{\underline{*}} = \underset{\boldsymbol{\theta} \in \boldsymbol{\theta}^I}{\operatorname{argmin}} \ \max_l ||A_{l:}(\boldsymbol{\theta})||_2 \tag{42}$$

$$\theta^{\overline{*}} = \underset{\boldsymbol{\theta} \in \boldsymbol{\theta}^I}{\operatorname{argmax}} \ \max_l ||A_{l:}(\boldsymbol{\theta})||_2 \tag{43}$$

In case more than one dynamic response $\eta_i(t, \boldsymbol{z}),\ i = 1, \ldots, n_\eta$ is considered, the optimization problem has to be expanded. Indeed, in this case a matrix A_i is defined for each response of interest, yielding following optimization problems:

$$\theta^{\underline{*}} = \underset{\boldsymbol{\theta} \in \boldsymbol{\theta}^I}{\operatorname{argmin}} \ \max_{i=1,\ldots,n_\eta} \ \max_l ||A_{i,l:}(\boldsymbol{\theta})||_2 \tag{44}$$

$$\theta^{\overline{*}} = \underset{\boldsymbol{\theta} \in \boldsymbol{\theta}^I}{\operatorname{argmax}} \ \max_{i=1,\ldots,n_\eta} \ \max_l ||A_{i,l:}(\boldsymbol{\theta})||_2 \tag{45}$$

In this equation, the maximal values of $\max_l ||A_{i,l:}(\boldsymbol{\theta})||_2$ over all responses $\eta_i(t, \boldsymbol{z}),\ i = 1, \ldots, n_\eta$ have to be considered jointly. Since usually only a limited number of dynamic responses are considered, the additional computational cost of the inner optimization is trivial.

These analyses show that the parameters of the stochastic ground acceleration model that yield the bounds on the first excursion probability of the structure can be determined in two optimization calls. Furthermore, this only requires a single deterministic call to the FE solver, namely to determine the impulse response functions h_i that are required to assemble $\boldsymbol{a}_{i,k}$, as shown in Eq. (10). Therefore, since the interval problem corresponding to Eq. (13) and Eq. (14) can be solved completely *a priori*, only 2

computations of the probability of failure are required:

$$\underline{P}_f = \int_{\boldsymbol{z}\in\mathbb{R}^{n_{KL}}} I_F\left(\boldsymbol{z}, \underline{\boldsymbol{\theta}^*}\right) f_{\boldsymbol{Z}}\left(\boldsymbol{z}\right) d\boldsymbol{z} \tag{46}$$

to obtain the lower bound and:

$$\overline{P}_f = \int_{\boldsymbol{z}\in\mathbb{R}^{n_{KL}}} I_F\left(\boldsymbol{z}, \overline{\boldsymbol{\theta}^*}\right) f_{\boldsymbol{Z}}\left(\boldsymbol{z}\right) d\boldsymbol{z} \tag{47}$$

to obtain the upper bound, strongly reducing the computational cost of the determination of the bounds on the first excursion probability of the structure subjected to an imprecise stochastic ground motion acceleration. As such, instead of having to solve $2 \times n_{opt} \times n_{P_f}$ solutions of Eq. (8), only $2 \times (n_{opt} + n_{P_f})$ solutions are required, where n_{opt} denotes the number of function calls performed by the optimization algorithm to solve the 'outer' loop, while n_{P_f} denotes the number of simulations required for determining the failure probability in the 'inner' loop.

5. Case study 1: Single-degree-of-freedom oscillator

5.1. Case introduction

This example comprises a single-degree-of-freedom oscillator with mass $m = 1$ kg, stiffness $k = 225$ N/m and classical damping $d = 5\%$ subject to a stochastic ground acceleration $g_A(t)$. The ground acceleration follows a modulated Clough-Penzien (CP) model. A description of this model along with the modulating function considered can be found in Appendix A. Nominal parameters for the modulated Clough-Penzien model are set equal to $[\omega_g, \omega_f, \zeta_g, \zeta_f, S_0, c_1, c_2] = [6\pi, 0.6\pi, 0.6, 0.6, 4 \times 10^{-2}, 0.14, 0.16]$. The total duration of the acceleration is 20 [s] and the time step discretization is $\Delta t = 0.01$ s. The prescribed threshold level is $b = 0.1$ m. The oscillator is at rest at the beginning of the stochastic excitation. The K-L expansion of the stochastic process is truncated at 99% of the total variance, yielding approximately 1300 terms in the expansion. The exact number of terms in the expansion depends on the actual parameter values in $\boldsymbol{\theta}^I$, and calculated for each stochastic process propagation run separately based on the variance truncation. Directional importance sampling with a sample size of 500 deterministic model evaluations is used to compute the crisp probability of failure. Using this set of parameters, the probability of failure of the mass-spring system is 0.0053 with a coefficient of variation of 0.0359.

To illustrate the performance of the developed approach, a study is performed with wide interval

widths on the parameters in $\boldsymbol{\theta}^I$, as illustrated in table 1. These bounds are derived from the data in table A.7 and expert knowledge and correspond to a case of nearly non-informative estimates on the parameters. For the soil conditions, parameters spanning the full range between Soft and Firm soil are considered. Due to the interval-valued definition of these parameters, also the probability of failure of the model will become interval valued. Furthermore, since the intervals on the parameters are wide, it is expected that the upper and lower bound on P_f will diverge also significantly.

Table 1: Tested values for $\boldsymbol{\theta}^I$

ω_g^I	ω_f^I	ζ_g^I	ζ_f^I	S_0^I	c_1^I	c_2^I
$\pi[2.4; 8]$	$\pi[0.24; 0.8]$	$[0.6; 0.85]$	$[0.6; 0.85]$	$4 \times 10^{-2}[0.75; 1.25]$	$[0.12; 0.16]$	$[0.14; 0.18]$

5.2. Computation of the bounds on P_f

The methods developed in this paper are applied to compute the bounds on P_f. Hereto, the operator norm that represents the magnitude of the amplification of the stochastic base excitation of the SDOF oscillator towards the maximally occurring displacement values is computed as:

$$||A(\boldsymbol{\theta})||_{p^{(1)}\to\infty, p^{(2)}=2} = \max_l ||\boldsymbol{A}_{l:}(\boldsymbol{\theta})||_2 \tag{48}$$

with $\boldsymbol{A} = \left[\boldsymbol{a}_1^T, \boldsymbol{a}_2^T, \ldots, \boldsymbol{a}_{n_T}^T\right]$ a matrix collecting the n_T vectors $\boldsymbol{a}_k$ (see eq. (10)) for each time instant t_k of the simulation. The parameter values of $\boldsymbol{\theta}^I$ that yield the bounds on P_f are then determined by solving Eq. (42) and Eq.(43). These optimization problems are solved using a sequential quadratic programming approach. Solving this equation leads to the intervals for the parameters $\boldsymbol{\theta}^{I,*} = [\underline{\boldsymbol{\theta}^*}; \overline{\boldsymbol{\theta}^*}]$ shown in table 3. The probability of failure corresponding to these two sets of hyper-parameters is then computed via Eq. (46) and Eq. (47). As such, only two calculations of the probability of failure are required, and hence, 1000 deterministic model evaluations. As can be noted from table 3, some values degenerate to a crisp number, indicating that both extremes of the maximum amplification of the signal, and hence, the probability of failure depend on the same vertex of $\boldsymbol{\theta}^I$. Furthermore, it may be noted that the upper bound on P_f depends on a value of ω_g^I that is located at neither bound.

To validate this approach, two additional methods for computing the bounds of P_f of the SDOF oscillator subjected to the imprecise stochastic load are applied: a vertex analysis and a double-loop Quasi Monte Carlo simulation. Both methods are aimed at replacing the 'outer' optimization loop in Eq. (13) and Eq. (14) by a computationally more efficient approximation.

The vertex analysis replaces the outer optimization in Eq. (13) and Eq. (14) by assessing all possible combinations of the bounds of the parameters in $\boldsymbol{\theta}^I$. For each of these combinations, a value for P_f is computed. Hence, $2^7 = 128$ computations of the probability of failure are required and hence, 64000 deterministic model evaluations.

The Quasi Monte Carlo simulation approach replaces the outer optimization problems by means of a quasi-random sampling scheme under the assumption of a uniform distribution between the bounds in $\boldsymbol{\theta}^I$. Following these auxilliary uniform distributions, a Sobol sequence with 500 points is generated and P_f is computed for each of these samples. This leads to 500 computations of the probability of failure and hence, 250000 deterministic model evaluations.

The results of these three propagation schemes are shown in Table 2. As can be noted, the bounds obtained by the optimization procedure are wider as compared to both the sets of bounds obtained via vertex analysis and Sobol sampling. Both the vertex analysis and Sobol sampling underestimate the upper bound on the probability of failure significantly. Furthermore, the lower bound of P_f as computed by both the optimization procedure and the vertex analysis is lower as compared to the one obtained by the Sobol set analysis. However, $\underline{P_f}$ as computed by the vertex analysis is lower as compared to the result of the Optimization procedure. This is explained by the results in table 3, which shows that the optimization method apparently derives the same value for the lower bound as the corresponding vertex. However, due to numerical precision of the optimizer, both values differ very slightly, and hence, small differences in the resulting failure probability exist, especially since the lower bound is extremely low. Increasing the numerical accuracy of the optimization algorithm that is used to solve Eq. (43) will alleviate this problem. Also from this table, it is clear that the problem is not necessarily monotonic with respect to the parameters of the CP model. Indeed, looking at the values that yield the upper bound, one can see that the value for ω_g that gives the highest probability of failure lies inside the interval. Since the vertex approach assumes monotonicity of all parameters with respect to P_f, it is not capable of determining the correct upper bound for the failure probability. The optimization approach introduced in this paper however, does not make assumptions on the monotonicity of P_f with respect to any parameters, and is therefore capable of determining the bounds exactly, at far reduced computational cost as compared to the other two methods. The origin of this non-monotonicity lies in the interplay between the frequency content of the non-stationary stochastic base excitation with resonances inside the structure. Since the optimization method takes this into account (see section 4), it is capable of tackling the non-monotonicity. This point is further clarified in figure 3, which shows the

Clough-Penzien power spectra corresponding to $\boldsymbol{\theta}^{\bar{*}}$, obtained by the Operator norm optimization method (O), Vertex sampling (V) and Sobol set propagation (S) together with the damped natural frequency of the SDOF oscillator (ω_d). As is clear, the dominant frequency of the CP spectrum corresponding to $\boldsymbol{\theta}^{\bar{*}}$ obtained via optimizing the operator norm perfectly matches with the damped eigenfrequency of the oscillator, which causes resonance, and hence, a higher probability of failure. This match with the eigenfrequency of the oscillator is not present in the two other spectra. It should be noted that this method only works when the considered structure is linear due to the inherent coupling with the solution of a dynamic linear system that underlies the derivations in section 4.

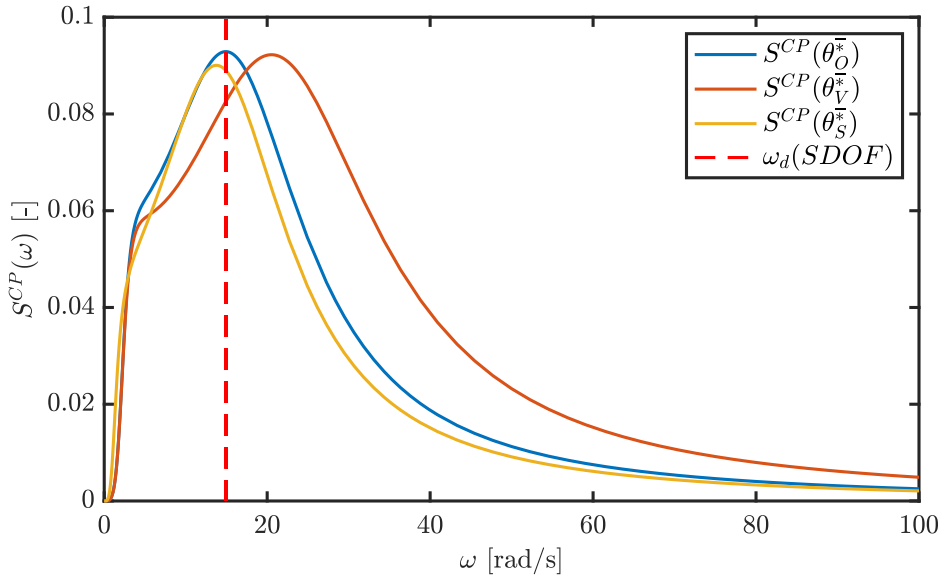

Figure 3: Clough-Penzien power spectra corresponding to $\boldsymbol{\theta}^{\bar{*}}$, obtained by the Operator norm optimization method (O), Vertex sampling (V) and Sobol set propagation (S).

Table 2: Computed bounds on the failure probability

	Vertex analysis	Sobol sampling	Optimization
P_f	$[2.77 \times 10^{-15}; 0.018]$	$[4.7 \times 10^{-14}; 0.0192]$	$[2.78 \times 10^{-15}; 0.328]$
$\max_l \|\|A_{l:}(\boldsymbol{\theta})\|\|_2$	$[0.01186; 0.0272]$	$[0.0123; 0.0279]$	$[0.0118; 0.0286]$

Table 3: Identified values for $\boldsymbol{\theta}^{I,*}$. O are the results from the optimization procedure, whereas V denotes the results from the vertex method. Note that the bounds on the reported intervals are those values that correspond to a bound on P_f.

Method	ω_g^I	ω_f^I	ζ_g^I	ζ_f^I	S_0^I	c_1^I	c_2^I
O	$\pi[2.4; 5.84]$	$\pi[0.8; 0.8]$	$[0.85; 0.6]$	$[0.85; 0.6]$	$4 \times 10^{-2}[0.75; 1.25]$	$[0.16; 0.12]$	$[0.18; 0.14]$
V	$\pi[2.4; 8]$	$\pi[0.8; 0.8]$	$[0.85; 0.6]$	$[0.85; 0.6]$	$4 \times 10^{-2}[0.75; 1.25]$	$[0.16; 0.12]$	$[0.18; 0.14]$

A further illustration of the results is given in figure 4. This figure shows the value of P_f plotted against $\max_l \|\|A_{l:}(\boldsymbol{\theta})\|\|_2$ for 500 Sobol samples in between the bounds of $\boldsymbol{\theta}^I$, combined with the data from

the vertex analysis. It can be noted that a monotonic relationship between these two quantities exists, and furthermore that the bounds on P_f indeed correspond to the bounds on $\max_l ||A_{l:}(\boldsymbol{\theta})||_2$. Finally, it can be noted that also a few Sobol samples lie outside the bounds provided by the vertex method (e.g., one around $\max_l ||A_{l:}(\boldsymbol{\theta})||_2 = 0.028$.

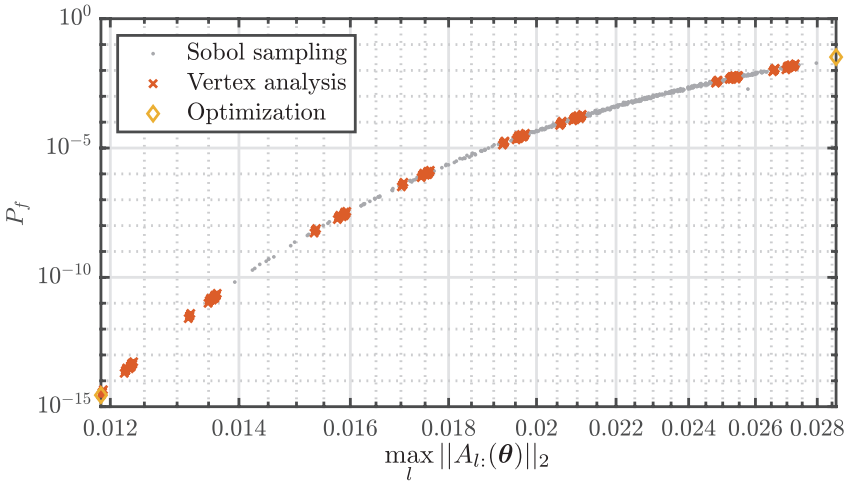

Figure 4: P_f plotted against $\max_l ||A_{l:}(\boldsymbol{\theta})||_2$ for 500 Sobol samples in between the bounds of $\boldsymbol{\theta}^I$, combined with the data from the vertex analysis

6. Case study 2: six story building model

6.1. Case introduction

The second example involves the six story reinforced concrete building model depicted in Figure 5, which is borrowed from [59]. Each floor plan is of square shape with side length 32 m and story height of 3.6 m. All floor slabs possess a thickness of 20 cm and are supported by a C-shaped shear wall of 20 cm thickness and 16 columns of square cross section with side length 40 cm. The Young's modulus is set equal to 2.3×10^{10} Pa. It is assumed that the building undergoes small displacements and hence, it is modeled as linear elastic. The behavior of the building is characterized by means of a finite element model that comprises about 9500 shell and beam elements and more than 50×10^3 degrees-of-freedom. The building is excited by a stochastic ground acceleration along the y direction. This ground acceleration is generated considering a modulated Clough-Penzien model, with nominal parameters $[\omega_g, \omega_f, \zeta_g, \zeta_f, S_0, c_1, c_2] = [4\pi, 0.4\pi, 0.7, 0.7, 3 \times 10^{-4}, 0.14, 0.16]$. Similarly to example 1, the stochastic process is truncated at 99 % of the total variance, yielding approximately 1300 terms in the KL expansion. The total duration of the acceleration is 20 s and the time step discretization is $\Delta t = 0.01$ s. Due to design purposes, it is of interest to control that the interstory drifts along the y

direction does not exceed a threshold level of 2×10^{-3} times the story height. These interstory drifts are controlled at five points, between nodes n_2-n_1, n_3-n_2, n_4-n_3, n_5-n_4 and n_6-n_5. The probability of failure is computed with Direction Importance Sampling with a sample size of 500 deterministic model evaluations. Table 4 illustrates the parameter interval on the parameters of the CP ground acceleration that is used to model the imprecision in the stochastic ground acceleration. Also in this case, due to the imprecision in the stochastic load, represented by the interval-valued definition of the governing hyper-parameters $\boldsymbol{\theta}$, the probability of failure will become interval-valued as well.

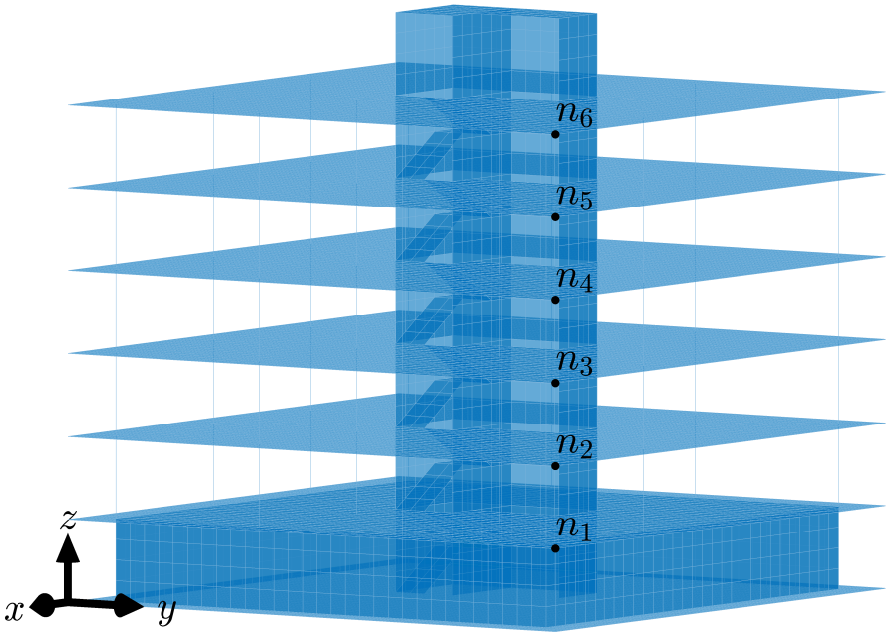

Figure 5: Example 2 – Isometric view of the building model

Table 4: Tested values for $\boldsymbol{\theta}^I$

ω_g^I	ω_f^I	ζ_g^I	ζ_f^I	S_0^I	c_1^I	c_2^I
$\pi[2.4; 8]$	$\pi[0.24; 0.8]$	$[0.6; 0.85]$	$[0.6; 0.85]$	$3 \times 10^{-4}[0.75; 1.25]$	$[0.12; 0.16]$	$[0.14; 0.18]$

6.2. Computation of the bounds on P_f

The results of these three propagation schemes are reported in table 5. First, it can be noted that the bounds produced by the Sobol sampling underestimate the width of the interval on P_f severely, where especially the underestimation of $\overline{P}_f$ is problematic. Furthermore, comparing the results of the vertex

analysis with the optimization procedure, it can be concluded that both predict the same bounds on the probability of failure. As such, in this case, the problem behaves seemingly monotonic with respect to $\boldsymbol{\theta}$.

Furthermore, despite the fact that the intervals on $\boldsymbol{\theta}^I$ are the same as in the case with the SDOF oscillator, the realizations that yield respectively $\underline{P}_f$ and $\overline{P}_f$ are completely different. For instance, concerning ω_g^I, the values that give $\underline{P}_f$ in the SDOF oscillator give $\overline{P}_f$ on the building model. This is due to the fact that the bounds of P_f are determined by both the energy content of the stochastic excitation, as well as the match of its dominant frequencies of the excitation with the resonances of the structure under consideration, especially when the latter are dominated by a few eigenmodes. Also this example shows that the proposed approach is capable of providing an analyst with a highly accurate estimation of the bounds on P_f within a very limited computational budget, as compared to a double loop approach. Especially the gain in computational efficiency is noteworthy, although the vertex analysis and optimization approach yield the same results concerning the bounds, the latter approach needs only $1 + 2 \times 500 = 1001$ deterministic model evaluations, whereas the former requires $128 \times 500 = 64000$ deterministic model evaluations, without any guarantee of conservatism in case the relation between $\boldsymbol{\theta}^I$ and P_f is not strictly monotonic.

Table 5: Computed bounds on the failure probability

	Vertex analysis	Sobol sampling	Optimization
P_f	$[4.47 \times 10^{-07}; 0.0495]$	$[1.14 \times 10^{-06}; 0.0275]$	$[4.47 \times 10^{-07}; 0.0495]$
$\max_i \max_l \lvert\lvert A_{i,l:}(\boldsymbol{\theta})\rvert\rvert_2$	$[9.44 \times 10^{-04}; 2.34 \times 10^{-03}]$	$[9.78 \times 10^{-04}; 2.21 \times 10^{-03}]$	$[9.44 \times 10^{-04}; 2.34 \times 10^{-03}]$

Table 6: Identified values for $\boldsymbol{\theta}^{I,*}$

Method	ω_g^I	ω_f^I	ζ_g^I	ζ_f^I	S_0^I	c_1^I	c_2^I
O	$\pi[8; 2.4]$	$\pi[0.8; 0.8]$	$[0.85; 0.6]$	$[0.85; 0.6]$	$3 \times 10^{-4}[0.75; 1.25]$	$[0.16; 0.12]$	$[0.18; 0.14]$
V	$\pi[8; 2.4]$	$\pi[0.8; 0.8]$	$[0.85; 0.6]$	$[0.85; 0.6]$	$3 \times 10^{-4}[0.75; 1.25]$	$[0.16; 0.12]$	$[0.18; 0.14]$

Finally, figure 6 shows the behavior of $\max_{i=1,\ldots,n_\eta} \max_l \lvert\lvert A_{i,l:}(\boldsymbol{\theta})\rvert\rvert_2$ with respect to P_f. Specifically, this figure shows the combined results of the optimization procedure, Sobol sampling and vertex analysis. It can be noted that also in this case a sufficiently convex optimization problem is obtained. However, the functional relation is comparably less smooth that in the case where only one response is considered. This is due to the additional optimization layer in Eq. (45).

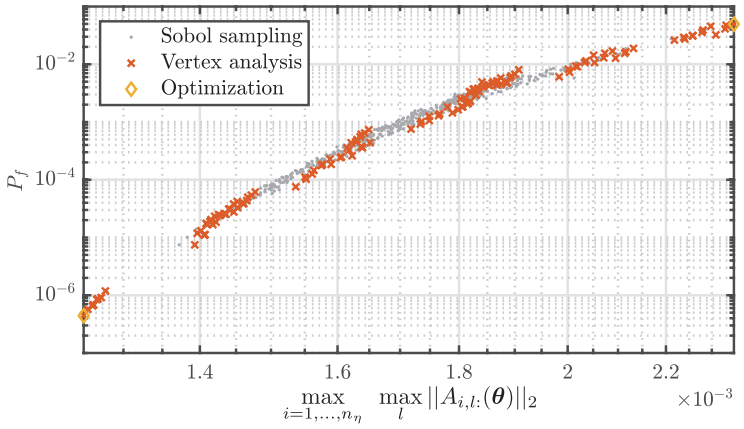

Figure 6: P_f plotted against $\max_{i=1,\ldots,n_\eta} \max_l ||A_{i,l:}(\boldsymbol{\theta})||_2$ for 500 Sobol samples in between the bounds of $\boldsymbol{\theta}^I$, combined with the data from the vertex analysis and the optimization procedure

7. Conclusions

This paper presents a highly efficient and accurate approach to determine the bounds on the first excursion probability of a linear oscillating system when the structure is excited by an imprecise stochastic process. The method decouples the epistemic uncertainty from the aleatory by *a priori* determining which parameters in the stochastic spectrum yield the bounds on the probability of failure of the structure. As such, the propagation of the epistemic uncertainty only requires a single deterministic model evaluation together with the solution of two optimization problems. The aleatory uncertainty in the problem is propagated using the framework of Directional Importance Sampling. Using the two parameter sets yielding the bounds on the probability of failure, only two Directional Importance Sampling evaluations are required.

The method is illustrated using the propagation of a non-stationary modulated Clough-Penzien excitation spectrum, but is generally applicable to the case of linear dynamical systems subjected to imprecise stochastic excitation. The conclusions of the paper can be summarized as follows:

- the proposed technique provides an extremely efficient approach to determine the bounds on the first excursion probability of a linear oscillator subjected to an imprecise stochastic excitation
- the method is shown to be more accurate than existing double loop approaches such as double loop quasi Monte Carlo
- since the method does not make assumptions on the monotonicity of the relationship of the probability of failure with the parameters of the exciting stochastic process, it is also more accurate than a combination of vertex analysis + directional importance sampling

Acknowledgment

The Research Foundation Flanders is gratefully acknowledged for the support of Matthias Faes under grant number 12P3519N. Marcos Valdebenito acknowledges the support of ANID (National Agency for Research and Development, Chile) under its program FONDECYT, grant number 1180271; Universidad Tecnica Federico Santa Maria under its program PAC (*Programa Asistente Cientifico 2017*); and the *Alexander von Humboldt Foundation* through its program *Humboldt Research Fellowship for Experienced Researchers*.

Appendix A. Clough-Penzien model

One of the most commonly used parametric models for the power spectral density associated with ground acceleration is the Kanai-Tajimi spectrum (see, e.g. [32]), whose physical basis consists of a white noise process of spectral intensity S_0 associated with the bedrock excitation that passes through a linear soil filter characterized in terms of a natural frequency ω_g and damping ζ_g. A drawback of the Kanai-Tajimi spectrum is that its associated velocity and displacement power spectra are not defined as the circular frequency tends to zero ($\omega \to 0$). Such issue is remedied by the Clough-Penzien power spectrum, which passes the signal produced by the Kanai-Tajimi spectrum through an additional linear filter with natural frequency ω_f and damping ζ_f. The expression for the Clough-Penzien power spectrum S^{CP} is given by [32, 60]:

$$S^{\mathrm{CP}}(\omega) = \frac{\omega_g^4 + \left(2\zeta_g\omega_g\omega\right)^2}{\left(\omega_g^2 - \omega^2\right)^2 + \left(2\zeta_g\omega_g\omega\right)^2} \cdot \frac{\omega^4}{\left(\omega_f^2 - \omega^2\right)^2 + \left(2\zeta_f\omega_f\omega\right)^2} \cdot S_0 \tag{A.1}$$

Typical values for the filter parameters associated with the Clough-Penzien power spectrum as suggested in [1] are shown in Table A.7. The autocorrelation function $R^{CP}(\tau)$ associated with the Clough-Penzien

Soil type	ω_g [rad/s]	ζ_g	ω_f [rad/s]	ζ_f
Firm	8π	0.60	0.8π	0.60
Medium	5π	0.60	0.5π	0.60
Soft	2.4π	0.85	0.24π	0.85

Table A.7: Filter parameters associated with Clough-Penzien power spectrum

power spectrum is calculated taking the inverse Fourier transform of S^{CP}, yielding [61]:

$$R^{\mathrm{CP}}(\tau) = \frac{\pi S_0}{2\zeta_g\omega_g} e^{-\zeta_g\omega_g|\tau|}\left((C_{a1}+C_{b1})\cos\left(\omega_g^d|\tau|\right) + \frac{\zeta_g\omega_g}{\omega_g^d}\left(C_{a1}-C_{b1}\right)\sin\left(\omega_g^d|\tau|\right)\right) \tag{A.2}$$

$$+ \frac{\pi S_0}{2\zeta_f\omega_f} e^{-\zeta_f\omega_f|\tau|}\left((C_{a2}+C_{b2})\cos\left(\omega_f^d|\tau|\right) + \frac{\zeta_f\omega_f}{\omega_f^d}\left(C_{a2}-C_{b2}\right)\sin\left(\omega_f^d|\tau|\right)\right) \tag{A.3}$$

where the constants ω_g^d, ω_f^d, C_{a1}, C_{a2}, C_{b1} and C_{b2} are defined as indicated below:

$$\omega_g^d = \sqrt{1-\zeta_g^2}\omega_g \tag{A.4}$$

$$\omega_f^d = \sqrt{1-\zeta_f^2}\omega_f \tag{A.5}$$

$$C_{a1} = -\frac{\omega_g^6}{D}\left(\left(1+8\zeta_g^2-16\zeta_g^4\right)\left(1-\frac{\omega_g^4}{\omega_f^4}\right) - 8\zeta_g^2\frac{\omega_g^2}{\omega_f^2}\left(1-2\zeta_f^2-\frac{\omega_g^2}{\omega_f^2}+2\zeta_g^2\frac{\omega_g^2}{\omega_f^2}\right)\right) \tag{A.6}$$

$$C_{b1} = \frac{2\omega_g^6}{D}\left(\left(1+8\zeta_g^2-16\zeta_g^4\right)\left(1-2\zeta_g^2-\frac{\omega_g^2}{\omega_f^2}+2\zeta_f^2\frac{\omega_g^2}{\omega_f^2}\right) - 2\zeta_g^2\left(1-\frac{\omega_g^4}{\omega_f^4}\right)\right) \tag{A.7}$$

$$C_{a2} = \frac{\omega_g^4\omega_f^2}{D}\left(\left(1+8\zeta_g^2-16\zeta_g^4\right)\left(1-\frac{\omega_g^4}{\omega_f^4}\right) - 8\zeta_g^2\frac{\omega_g^2}{\omega_f^2}\left(1-2\zeta_f^2-\frac{\omega_g^2}{\omega_f^2}+2\zeta_g^2\frac{\omega_g^2}{\omega_f^2}\right)\right) \tag{A.8}$$

$$C_{b2} = \frac{2\omega_g^2\omega_f^4}{D}\left(\frac{\omega_g^2}{\omega_f^2}\left(-\frac{\omega_g^2}{\omega_f^2}-8\zeta_g^2+16\zeta_g^2\zeta_f^2\right)\left(1-2\zeta_g^2-\frac{\omega_g^2}{\omega_f^2}+2\zeta_f^2\frac{\omega_g^2}{\omega_f^2}\right) + 2\zeta_g^2\left(1-\frac{\omega_g^4}{\omega_f^4}\right)\right) \tag{A.9}$$

$$D = -4\omega_g^2\omega_f^2\left(1-2\zeta_g^2-\frac{\omega_g^2}{\omega_f^2}+2\zeta_f^2\frac{\omega_g^2}{\omega_f^2}\right)\left(1-2\zeta_f^2-\frac{\omega_g^2}{\omega_f^2}+2\zeta_g^2\frac{\omega_g^2}{\omega_f^2}\right) + \omega_f^4\left(1-\frac{\omega_g^4}{\omega_f^4}\right) \tag{A.10}$$

The above discussion assumes that the ground acceleration can be modeled as a wide-sense stationary stochastic process. It is clear that this is a simplifying assumption, as ground acceleration exhibits a non stationary behavior. A possible means for including such effect in the Clough-Penzien model consists of modulating the white noise bedrock process by means of a deterministic function of time $m(t)$ (see, e.g. [33]). Here, the so-called Shinozuka and Sato modulating function [2] is considered:

$$m(t) = \frac{1}{c_3}\left(e^{-c_1 t} - e^{-c_2 t}\right) \tag{A.11}$$

where c_1 and c_2 are parameters of the model and c_3 is defined such that the maximum value of the modulating function is equal to unity, yielding:

$$c_3 = \frac{c_1}{c_2-c_1} e^{\frac{c_2}{c_2-c_1}\ln\left(\frac{c_2}{c_1}\right)} \tag{A.12}$$

References

[1] G. Deodatis, Non-stationary stochastic vector processes: seismic ground motion applications, Probabilistic Engineering Mechanics 11 (3) (1996) 149 – 167. doi:https://doi.org/10.1016/0266-8920(96)00007-0.
URL http://www.sciencedirect.com/science/article/pii/0266892096000070

[2] M. Shinozuka, Y. Sato, Simulation of nonstationary random process, Journal of the Engineering Mechanics Division 93 (1) (1967) 11–40.

[3] M. Beer, Y. Zhang, S. T. Quek, K. K. Phoon, Reliability analysis with scarce information: Comparing alternative approaches in a geotechnical engineering context, Structural Safety 41 (2013) 1–10. doi:10.1016/j.strusafe.2012.10.003.
URL http://dx.doi.org/10.1016/j.strusafe.2012.10.003

[4] M. Beer, S. Ferson, V. Kreinovich, Imprecise probabilities in engineering analyses, Mechanical Systems and Signal Processing 37 (1-2) (2013) 4–29. doi:http://dx.doi.org/10.1016/j.ymssp.2013.01.024.
URL http://www.sciencedirect.com/science/article/pii/S0888327013000812

[5] D. Moens, D. Vandepitte, An interval finite element approach for the calculation of envelope frequency response functions, International Journal for Numerical Methods in Engineering 61 (14) (2004) 2480–2507. doi:10.1002/nme.1159.
URL http://dx.doi.org/10.1002/nme.1159

[6] M. Faes, G. D. Sabyasachi, D. Moens, Hybrid spatial uncertainty analysis for the estimation of imprecise failure probabilities in laser sintered pa-12 parts, Computers & Mathematics with Applications 78 (7) (2019) 2395 – 2406, simulation for Additive Manufacturing. doi:https://doi.org/10.1016/j.camwa.2018.08.056.
URL http://www.sciencedirect.com/science/article/pii/S0898122118304826

[7] W. Gao, D. Wu, C. Song, F. Tin-Loi, X. Li, Hybrid probabilistic interval analysis of bar structures with uncertainty using a mixed perturbation monte-carlo method, Finite Elements in Analysis and Design 47 (7) (2011) 643–652.

[8] B. Xia, D. Yu, J. Liu, Hybrid uncertain analysis for structural-acoustic problem with random and interval parameters, Journal of Sound and Vibration 332 (11) (2013) 2701–2720. doi:10.1016/j.jsv.2012.12.028.

[9] S. Yin, D. Yu, Z. Luo, B. Xia, Unified polynomial expansion for interval and random response analysis of uncertain structure-acoustic system with arbitrary probability distribution, Computer Methods in Applied Mechanics and Engineering 336 (2018) 260 – 285. doi:https://doi.org/10.1016/j.cma.2018.03.014.
URL http://www.sciencedirect.com/science/article/pii/S0045782518301397

[10] M. Faes, D. Moens, Recent Trends in the Modeling and Quantification of Non-probabilistic Uncertainty, Archives of Computational Methods in Engineering (feb 2019). doi:10.1007/s11831-019-09327-x.
URL https://doi.org/10.1007/s11831-019-09327-x

[11] J. Wu, Z. Luo, Y. Zhang, N. Zhang, L. Chen, Interval uncertain method for multibody mechanical systems using Chebyshev inclusion functions, International Journal for Numerical Methods in Engineering 95 (7) (2013) 608–630. doi:10.1002/nme.4525.

[12] R. Schöbi, B. Sudret, Structural reliability analysis for p-boxes using multi-level meta-models, Probabilistic Engineering Mechanics 48 (2017) 27–38. doi:https://doi.org/10.1016/j.probengmech.2017.04.001.
URL http://www.sciencedirect.com/science/article/pii/S0266892017300152

[13] R. Schöbi, B. Sudret, Global sensitivity analysis in the context of imprecise probabilities (p-boxes) using sparse polynomial chaos expansions, Reliability Engineering & System Safety 187 (2019) 129 – 141, sensitivity Analysis of Model Output. doi:https://doi.org/10.1016/j.ress.2018.11.021.
URL http://www.sciencedirect.com/science/article/pii/S0951832017306099

[14] M. Faes, J. Sadeghi, M. Broggi, M. de Angelis, E. Patelli, M. Beer, D. Moens, On the Robust Estimation of Small Failure Probabilities for Strong Nonlinear Models, ASCE-ASME J Risk and Uncert in Engrg Sys Part B Mech Engrg 5 (4) (dec 2019). doi:10.1115/1.4044044.
URL https://asmedigitalcollection.asme.org/risk/article/doi/10.1115/1.4044044/955249/On-t

[15] J. Sadeghi, M. de Angelis, E. Patelli, Robust propagation of probability boxes by interval predictor

models, Structural Safety 82 (2020) 101889. doi:https://doi.org/10.1016/j.strusafe.2019.101889.
URL http://www.sciencedirect.com/science/article/pii/S0167473018303035

[16] P. Wei, J. Song, S. Bi, M. Broggi, M. Beer, Z. Lu, Z. Yue, Non-intrusive stochastic analysis with parameterized imprecise probability models: I. performance estimation, Mechanical Systems and Signal Processing 124 (2019) 349 – 368. doi:https://doi.org/10.1016/j.ymssp.2019.01.058.
URL http://www.sciencedirect.com/science/article/pii/S0888327019300743

[17] P. Wei, J. Song, S. Bi, M. Broggi, M. Beer, Z. Lu, Z. Yue, Non-intrusive stochastic analysis with parameterized imprecise probability models: II. reliability and rare events analysis, Mechanical Systems and Signal Processing 126 (2019) 227 – 247. doi:https://doi.org/10.1016/j.ymssp.2019.02.015.
URL http://www.sciencedirect.com/science/article/pii/S0888327019300986

[18] J. Hurtado, D. Alvarez, J. Ramirez, Fuzzy structural analysis based on fundamental reliability concepts, Computers & Structures 112–113 (2012) 183–192. doi:10.1016/j.compstruc.2012.08.004.

[19] M. Troffaes, Imprecise monte carlo simulation and iterative importance sampling for the estimation of lower previsions, International Journal of Approximate Reasoning 101 (2018) 31 – 48. doi:https://doi.org/10.1016/j.ijar.2018.06.009.
URL http://www.sciencedirect.com/science/article/pii/S0888613X17305868

[20] W. Gao, D. Wu, K. Gao, X. Chen, F. Tin-Loi, Structural reliability analysis with imprecise random and interval fields, Applied Mathematical Modelling 55 (2018) 49–67. doi:https://doi.org/10.1016/j.apm.2017.10.029.
URL https://www.sciencedirect.com/science/article/pii/S0307904X17306467

[21] M. Dannert, A. Fau, R. Fleury, M. Broggi, U. Nackenhorst, M. Beer, A probability-box approach on uncertain correlation lengths by stochastic finite element method, PAMM (Proceedings in Applied Mathematics and Mechanics) 18 (1) (2018) e201800114. arXiv:https://onlinelibrary.wiley.com/doi/pdf/10.1002/pamm.201800114, doi:10.1002/pamm.201800114.
URL https://onlinelibrary.wiley.com/doi/abs/10.1002/pamm.201800114

[22] M. Faes, D. Moens, Imprecise random field analysis with parametrized kernel functions, Mechanical Systems and Signal Processing 134 (2019) 106334. doi:10.1016/j.ymssp.2019.106334.

[23] L. Comerford, H. Jensen, F. Mayorga, M. Beer, I. Kougioumtzoglou, Compressive sensing with an adaptive wavelet basis for structural system response and reliability analysis under missing data, Computers & Structures 182 (2017) 26–40. doi:10.1016/j.compstruc.2016.11.012.
URL //www.sciencedirect.com/science/article/pii/S0045794916304618

[24] S. Montoya-Noguera, T. Zhao, Y. Hu, Y. Wang, K.-K. Phoon, Simulation of non-stationary non-gaussian random fields from sparse measurements using bayesian compressive sampling and Karhunen-Loève expansion, Structural Safety 79 (2019) 66 – 79. doi:https://doi.org/10.1016/j.strusafe.2019.03.006.
URL http://www.sciencedirect.com/science/article/pii/S0167473018303266

[25] Y. Zhang, L. Comerford, I. A. Kougioumtzoglou, E. Patelli, M. Beer, Uncertainty Quantification of Power Spectrum and Spectral Moments Estimates Subject to Missing Data, ASCE-ASME Journal of Risk and Uncertainty in Engineering Systems, Part A: Civil Engineering 3 (4) (2017) 04017020. doi:10.1061/ajrua6.0000925.

[26] M. Misraji, M. Valdebenito, H. Jensen, C. Mayorga, Application of directional importance sampling for estimation of first excursion probabilities of linear structural systems subject to stochastic Gaussian loading, Mechanical Systems and Signal Processing 139 (2020) 106621. doi:https://doi.org/10.1016/j.ymssp.2020.106621.
URL http://www.sciencedirect.com/science/article/pii/S0888327020300078

[27] A. Chopra, Dynamics of structures: theory and applications to earthquake engineering, Prentice Hall, 1995.

[28] A. Giaralis, P. Spanos, Derivation of response spectrum compatible non-stationary stochastic processes relying on Monte Carlo-based peak factor estimation, Earthquakes and Structures 3 (3) (2012) 581–609.

[29] G. Housner, Characteristics of strong-motion earthquakes, Bulletin of the Seismological Society of America 37 (1) (1947) 19–31, cited By 141.

[30] J. Hurtado, Modelación estocástica de la acción sísmica, no. Monografía CIMNE IS-33, Centro Internacional de Métodos Numéricos en Ingeniería, 1999.

[31] V. Papadopoulos, D. Giovanis, Stochastic Finite Element Methods, Springer, Cham, 2018. doi:10.1007/978-3-319-64528-5.

[32] T. Soong, M. Grigoriu, Random Vibration of Mechanical and Structural Systems, Prentice Hall, Englewood Cliffs, New Jersey, 1993.

[33] C.-H. Yeh, Y. Wen, Modeling of nonstationary ground motion and analysis of inelastic structural response, Structural Safety 8 (1-4) (1990) 281–298.

[34] J. Li, J. Chen, Stochastic Dynamics of Structures, John Wiley & Sons, Singapore, 2009. doi:10.1002/9780470824269.

[35] C. Schenk, G. Schuëller, Uncertainty Assessment of Large Finite Element Systems, Springer-Verlag, Berlin/Heidelberg/New York, 2005.

[36] G. Stefanou, The stochastic finite element method: Past, present and future, Computer Methods in Applied Mechanics and Engineering 198 (9-12) (2009) 1031–1051.

[37] J. Lee, M. Verleysen, Nonlinear Dimensionality Reduction, Springer, 2007.

[38] W. Betz, I. Papaioannou, D. Straub, Numerical methods for the discretization of random fields by means of the Karhunen-Loève expansion, Computer Methods in Applied Mechanics and Engineering 271 (2014) 109–129. doi:10.1016/j.cma.2013.12.010.
URL http://dx.doi.org/10.1016/j.cma.2013.12.010

[39] W. Gautschi, Numerical Analysis, 2nd Edition, Birkhäuser Boston, 2012. doi:10.1007/978-0-8176-8259-0.

[40] S. Au, J. Beck, Estimation of small failure probabilities in high dimensions by subset simulation, Probabilistic Engineering Mechanics 16 (4) (2001) 263–277.

[41] K. Marti, Differentiation of probability functions: The transformation method, Computers & Mathematics with Applications 30 (3-6) (1995) 361–382.

[42] Y. Zhang, A. Der Kiureghian, First-excursion probability of uncertain structures, Probabilistic Engineering Mechanics 9 (1-2) (1994) 135–143.

[43] K. Marti, Approximation and derivatives of probabilities of survival in structural analysis and design, Structural Optimization 13 (4) (1997) 230–243.

[44] A. A. Taflanidis, J. Beck, Analytical approximation for stationary reliability of certain and uncertain linear dynamic systems with higher-dimensional output, Earthquake Engineering & Structural Dynamics 35 (10) (2006) 1247–1267. doi:10.1002/eqe.581.

[45] G. Schuëller, H. Pradlwarter, Benchmark study on reliability estimation in higher dimensions of structural systems – An overview, Structural Safety 29 (2007) 167–182.

[46] S.-S. Lai, Statistical characterization of strong ground motions using power spectral density function, Bulletin of the Seismological Society of America 72 (1) (1982) 259–274.

[47] L. G. Crespo, D. P. Giesy, S. P. Kenny, Interval predictor models with a formal characterization of uncertainty and reliability, Proceedings of the IEEE Conference on Decision and Control 2015-Febru (February) (2014) 5991–5996. doi:10.1109/CDC.2014.7040327.

[48] M. Imholz, M. Faes, D. Vandepitte, D. Moens, Robust uncertainty quantification in structural dynamics under scarse experimental modal data: A bayesian-interval approach, Journal of Sound and Vibration 467 (2020) 114983. doi:https://doi.org/10.1016/j.jsv.2019.114983.
URL http://www.sciencedirect.com/science/article/pii/S0022460X19305450

[49] M. Faes, J. Sadeghi, M. Broggi, M. de Angelis, E. Patelli, M. Beer, D. Moens, On the Robust Estimation of Small Failure Probabilities for Strong Nonlinear Models, ASCE-ASME J Risk and Uncert in Engrg Sys Part B Mech Engrg 5 (4) (dec 2019). doi:10.1115/1.4044044.

[50] O. Ditlevsen, R. Olesen, G. Mohr, Solution of a class of load combination problems by directional simulation, Structural Safety 4 (2) (1987) 95–109.

[51] P. Bjerager, Probability integration by directional simulation, Journal of Engineering Mechanics 114 (8) (1988) 1285–1297.

[52] O. Ditlevsen, P. Bjerager, R. Olesen, A. Hasofer, Directional simulation in Gaussian processes, Probabilistic Engineering Mechanics 3 (4) (1988) 207 – 217. doi:https://doi.org/10.1016/0266-8920(88)90013-6.
URL http://www.sciencedirect.com/science/article/pii/0266892088900136

[53] A. Ang, W. Tang, Probability Concepts in Engineering: Emphasis on Applications to Civil and Environmental Engineering, Wiley, 2007.
URL https://books.google.cl/books?id=G4IoAQAAMAAJ

[54] A. Der Kiureghian, The geometry of random vibrations and solutions by FORM and SORM, Probabilistic Engineering Mechanics 15 (1) (2000) 81–90.

[55] S. Au, J. Beck, First excursion probabilities for linear systems by very efficient importance sampling, Probabilistic Engineering Mechanics 16 (3) (2001) 193–207.

[56] G. Schuëller, R. Stix, A critical appraisal of methods to determine failure probabilities, Structural Safety 4 (4) (1987) 293–309.

[57] L. Katafygiotis, S. Cheung, Domain decomposition method for calculating the failure probability of linear dynamic systems subjected to Gaussian stochastic loads, Journal of Engineering Mechanics 132 (5) (2006) 475–486.

[58] J. Tropp, Topics in sparse approximation, Ph.D. thesis, The University of Texas at Austin (2004).

[59] E. Patelli, H. Panayirci, M. Broggi, B. Goller, P. Beaurepaire, H. Pradlwarter, G. Schuëller, General purpose software for efficient uncertainty management of large finite element models, Finite Elements in Analysis and Design 51 (2012) 31–48. doi:10.1016/j.finel.2011.11.003.

[60] A. Zerva, Spatial Variation of Seismic Ground Motions – Modeling and Engineering Applications, CRC Press, 2009.

[61] G. Fu, Seismic response statistics of SDOF system to exponentially modulated coloured input: An explicit solution, Earthquake Engineering & Structural Dynamics 24 (10) (1995) 1355–1370. doi:10.1002/eqe.4290241006.
URL https://onlinelibrary.wiley.com/doi/abs/10.1002/eqe.4290241006